Theoretical investigation of the distance dependence of capillary and van der Waals forces in scanning force microscopy

Thomas Stifter*
Department of Experimental Physics, University of Ulm, 89069 Ulm, Germany

Othmar Marti
Department of Experimental Physics, University of Ulm, 89069 Ulm, Germany

Bharat Bhushan
Department of Mechanical Engineering, Ohio State University, Columbus, Ohio 43210
(Received 19 May 2000)

The capillary and van der Waals forces between a tip and a plane in a scanning force microscope (SFM) are calculated. The forces are calculated for a fixed distance of tip and sample, as well as during retracting of the tip from the sample surface. The exact geometric shape of the meniscus is considered, with the boundary condition of fixed liquid volume during retraction. The starting volume is given by the operating and environmental conditions (surface tension, humidity, and tip geometry) at the point of lowest distance between tip and surface. The influence of the different parameters, namely, humidity, tip geometry, tip-sample starting distance, surface tension, and contact angles are studied. For each force curve also the geometric shape of the meniscus is calculated. The capillary forces are compared with van der Waals forces to understand their relative importance in various operating conditions. In addition to application in SFM, this analysis is useful in the design of surface roughness in microdevices for low adhesion in operating environments.

I. INTRODUCTION

With the invention of the scanning force microscope (SFM) in 1986 by Binnig *et al.*[1] a powerful probe for a variety of surface studies was made available.[2,3] An important property of the SFM is its ability to investigate various sample properties such as adhesion,[4] surface charge,[5] and magnetic properties[6] on a nanometer scale. However, if the SFM is operating in air, capillary forces of water films or other liquids cause a strong interaction between the tip and sample. The adhesion, which is the force necessary to separate the tip from the sample, changes with the presence of the liquid film.[7–9] Since the introduction of SFM modes such as the force volume mode,[10] pulsed force mode,[11,12] and jumping mode,[13] the adhesion can be easily obtained with high lateral resolution. The capillary forces depend on the liquid volume and its properties and on the interface geometry including the SFM tip radius. Dependent upon the interface conditions, the capillary forces can be large as compared to weak van der Waals forces. For lightly loaded conditions, these forces may be comparable to external load. The adhesion due to capillary forces plays also an important role in producing and the working of microelectromechanical systems[2,3,14,15] (MEMS). Therefore results of this study can be used to design a model of surface roughness for low adhesion.

In SFM, not only the force at the contact is needed to study the influence of capillary forces on adhesion, but the distance dependence starting from contact until the break of the meniscus between tip and sample is necessary for an investigation. In this paper we present an analysis to obtain the distance dependence of the meniscus force between a SFM tip and a surface. The tip is represented by a parabolic shaped tip and the surface is a half plane. The influence of the different parameters is presented. In the latter part of the paper, the capillary forces are compared to van der Waals forces and their relative importance in various operating conditions is studied.

II. ANALYSIS OF CAPILLARY AND VAN DER WAALS FORCES

A. Capillary forces

Liquids can spontaneously condense from the vapor phase to the liquid state at small cracks and pores. The reason for the capillary condensation lies in the pressure difference across the interface of a curved surface,

$$p=\gamma\left(\frac{1}{r_1}+\frac{1}{r_2}\right), \tag{1}$$

where γ is the surface tension and r_1 and r_2 are the two principal radii of the curved surface. This equation is often called the Young-Laplace equation.[3,16,17] From the thermodynamic view the pressure difference influences the free molar energy. The change in free molar energy at constant temperature and a molar volume V caused by a change in the pressure is given by

$$\Delta G=V\Delta p. \tag{2}$$

Combining the Young-Laplace equation (1) to describe the pressure difference and the relation for the ideal free molar energy we get

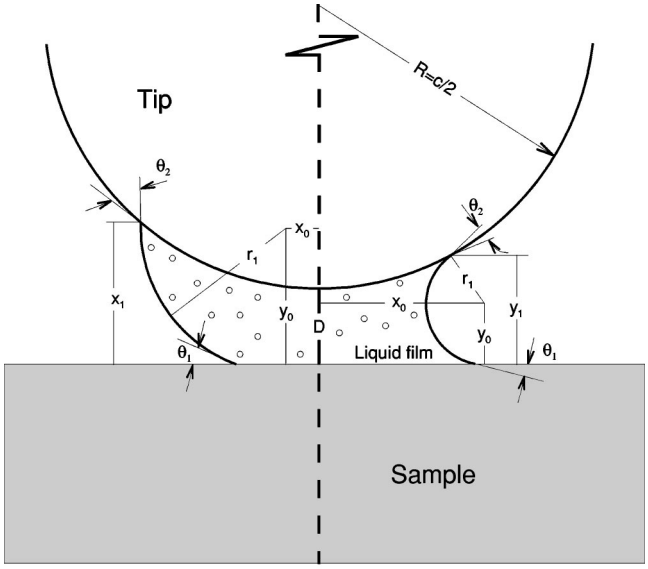

FIG. 1. Schematic of a sphere on a plane at distance D with a liquid film in between, forming concave- (right) and convex- (left) shaped menisci.

$$RT\ln\frac{p}{p_0}=\gamma V\left(\frac{1}{r_1}+\frac{1}{r_2}\right), \tag{3}$$

where R is the universal gas constant, T the absolute temperature, p_0 the normal vapor pressure of the liquid, and p the pressure acting outside the curved surface. Equation (3) is generally called the Kelvin equation. At given environment parameters (T, γ, V, and p/p_0) the Kelvin equation provides the so-called Kelvin radius

$$r_k^{-1}=\left(\frac{1}{r_1}+\frac{1}{r_2}\right)=\frac{RT}{\gamma V}\ln\frac{p}{p_0}. \tag{4}$$

This radius defines for the given parameters the adjustable curvature of the condensing liquid. Thus, the relative vapor pressure p/p_0 plays an important role and the water film present from capillary condensation is a direct consequence of the relative humidity. To calculate now the force acting on a SFM tip, the capillary condensation in the case of a smooth sphere on a smooth plane is considered (Fig. 1). With the Young-Laplace equation (1) for the pressure difference and the area πx^2 the force working/acting perpendicular to this area is given as

$$F=p\,\pi x^2=\gamma\left(\frac{1}{r_1}+\frac{1}{r_2}\right)\pi x^2. \tag{5}$$

For a liquid film that wets the tip, the meniscus formed is concave in shape as shown in Fig. 1. A concave meniscus with a negative radius of curvature results in an attractive force between the SFM tip and the surface. In most cases of interest $r_2 \gg r_1$; thus F in Eq. (5) becomes negative, meaning that it acts towards the surface. Nevertheless the meniscus force does not act at all distances, because it appears on the approach only at or shortly before contact. Retracting of the tip results in breakage of the capillary, thus elimination of the meniscus force, at a significant distance from the surface.

To calculate the meniscus forces for each separation of the tip and the surface, the geometric shape of the meniscus has to be determined. The starting point is the Kelvin radius [Eq. (3)] and the force between tip and surface [Eq. (5)]. Figure 1 shows the schematic of a SFM tip in contact with a plane surface for concave- and convex-shaped menisci. For calculating the meniscus force between the tip and the surface the two radii r_1 and r_2 of Eq. (5) must be known. To get the two radii the surface of the liquid is described by two intersections. The first intersection, in-plane vertical to the surface, is represented by an arc, and the second, in-plane parallel to the surface, is described by a circle. The two radii are distinguished as follows: r_1 is the radius of arc and r_2 is approximately the distance of the midpoint x_0 from the rotation axis minus the radius r_1 of the arc: $r_2=x_0-r_1$. In the following model the y axis lies normal to the surface. The origin of the coordinate system is at the point of intersection of the rotating axis with the surface. Therefore the general equation for the arc is given by

$$x(y)=x_0\pm\sqrt{r_1^2-(y-y_0)^2} \tag{6}$$

with the positive sign for an arc for the convex case in the left part of Fig. 1 and the negative sign for the concave case.

First the concave case will be investigated. To distinguish the midpoint (x_0,y_0) and the radius r_1 of the circle part, the following boundary conditions must be considered:

$$\left.\frac{dy(x)}{dx}\right|_{y=0}=-\alpha_1,$$

$$y(x)\big|_{y_1}\in\mathbf{P}=\left\{x\,\middle|\,y_{\mathbf{p}}(x)=\frac{x^2}{c}+D\right\}, \tag{7}$$

$$\left.\frac{dy(x)}{dx}\right|_{y_1}=\frac{\left.\frac{dy_{\mathbf{p}}(x)}{dx}\right|_{y_1}-\alpha_2}{1-\left.\frac{dy_{\mathbf{p}}(x)}{dx}\right|_{y_1}\alpha_2},$$

where $\alpha_1=\tan\theta_1$ and $\alpha_2=\tan\theta_2$ with θ_1 and θ_2 being the contact angle of the liquid at the surface and the tip, respectively. The set $\mathbf{P}$ defines the shape of the tip. Here it is a parabola with the parameter c as an intersection of the paraboloid shaped tip. If the parabola approximated by a circle with the radius R the relation $c=2R$ holds. The solution for the midpoint (x_0,y_0) and the radius r_1 due to the three boundary conditions is not unique, e.g., y_1 can be freely chosen. The distance D cannot be chosen freely because the force shall be calculated for this fixed distance. To get a unique solution the Kelvin radius from Eq. (3) for a given liquid $(\gamma,\theta_1,\theta_2,V)$ an additional boundary condition at $D=z_0$ is used:

$$\frac{1}{r_1}+\frac{1}{y_0-r_1}=r_k^{-1}. \tag{8}$$

The distance z_0 is the closest approach of the tip, meaning at this distance the meniscus is built and then the tip is retracted. With this determined arc it is possible with Eq. (5) to calculate the force between the tip and the surface and also the volume of the liquid collected under the tip. This volume will be kept constant for distances $D>z_0$ between tip and

surface and replaces the boundary condition Eq. (8) in this case. Finally the disappearance of the meniscus forces must be determined. This is the case for $x_0 = r_1$, because for this condition the neck is zero and the meniscus is no longer formed, meaning the meniscus breaks.

The second meniscus shape, the convex case (left side of Fig. 1), uses the same boundary conditions (7) and (8) as the concave constellation. There are, however, only a few special cases where a solution for the boundary conditions are found. The reason is due to the Kelvin radius, in that the geometry of a concave-shaped meniscus is not treated by the boundary condition (8). This is the reason why the following calculations are only done for the concave condition.

The force acting between tip and surface is calculated by Eq. (5) with $x = x_0 - r_1$ and $r_2 = x_0 - r_1$:

$$F = \gamma\pi(x_0 - r_1)^2\left(\frac{1}{-r_1} + \frac{1}{x_0 - r_1}\right). \tag{9}$$

Due to the shape the radius r_1 has to be considered negative. For small distances between tip and surface $r_1 \ll x_0 - r_1$ and the force (9) is attractive.

B. van der Waals forces

In a SFM the capillary force is not the only force that occurs. A major force interacting between tip and sample in dry conditions is the Lennard-Jones force.[16,18,19] The Lennard-Jones force is styled as a classical macroscopic law versus a discrete atomic law, because this force allows us to describe the same scales of tip-surface distances and geometries as necessary for the capillary force. In general atomic laws can also deal with such a configuration, but the necessary computational input is larger. However, the results of both methods are principally equal.

For a better interpretation of how the capillary force will influence the tip-sample interaction, we need to consider the meniscus force as well as the Lennard-Jones force. The Lennard-Jones potential is composed of two interactions: the van der Waals attraction and the Pauli repulsion. The general expression for two interacting atoms is

$$V(\mathbf{r}) = -4\epsilon\left[\left(\frac{\sigma}{r}\right)^6 - \left(\frac{\sigma}{r}\right)^{12}\right] = -\frac{a}{r^6} + \frac{b}{r^{12}}, \tag{10}$$

with ϵ the depth of the minimum potential, σ the position of potential minimum, and the potential parameters $a = 4\epsilon\sigma^6$ and $b = 4\epsilon\sigma^{12}$. The second form allows a separation of attractive and repulsive part. van der Waals forces are of great significance, because they are always present and cannot be turned off.[16,20]

The repulsive part of the Lennard-Jones interaction considers only the Pauli exclusion principle, which is the repulsion caused by the overlap of the electron clouds of the two atoms. The quantum mechanical calculation for the resulting potential of the overlap of the wave functions yields an exponential dependence. Usually the exponential dependence is approximated by a power law with $n \gg 9$. For the Lennard-Jones potential $n = 12$ is chosen. The distance dependence of the repulsive part is given as square of the attractive part.

To get the interaction potential for a SFM system represented by a parabolic tip above a half plane, the atomic potential has to be integrated over the volume of the tip and sample. The calculation results in the potential[21]

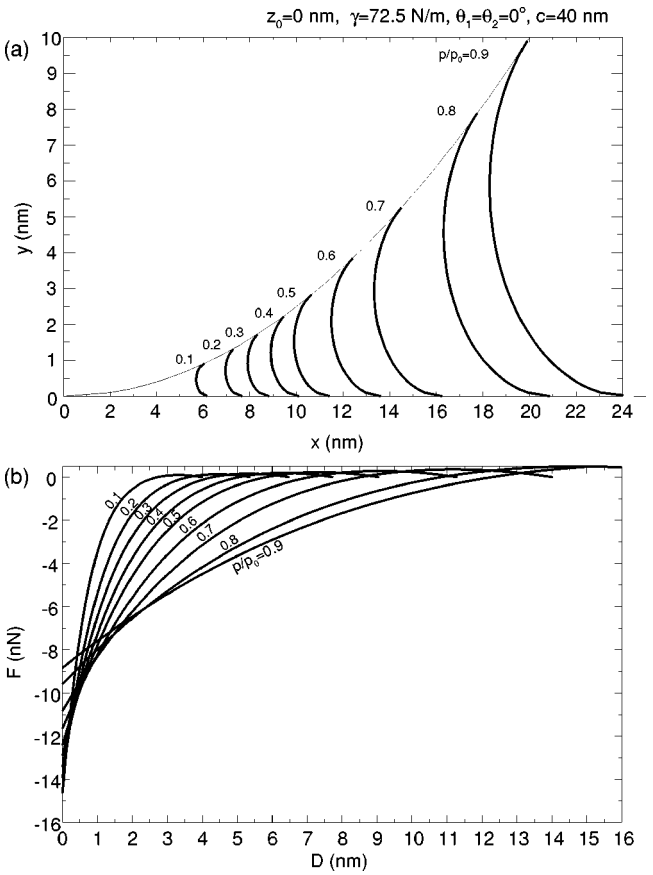

FIG. 2. (a) The upper diagram shows the geometric shape of the meniscus for $D = 0$ nm for various humidities p/p_0, and (b) the lower diagram shows the meniscus force between the tip and the surface.

$$V(D) = \frac{c}{12}\left(-\frac{A}{D} + \frac{B}{210\,D^7}\right), \tag{11}$$

with D the distance between tip and plane, c the width of the parabolic tip, and the two potential parameters $A = \pi^2 n_1 n_2 a$ and $B = \pi^2 n_1 n_2 b$. The constant A is the Hamaker constant.

III. RESULTS AND DISCUSSION

A. Capillary forces

Figure 2 shows the influence of different humidities on the meniscus forces. The lower diagram shows the force curves and the upper diagram the geometric shapes of the meniscus between the tip and the surface for the distance $D = z_0$. The force curve for the lowest humidity has the greatest force value at z_0, the strongest distance dependency, and the earliest point where the force disappears. With increasing humidity the force value at z_0 gets smaller, the distance dependency gets weaker, and the point when disappearance occurs lengthens. This behavior is expected for increasing humidity, because a higher humidity means a greater Kelvin radius, thus decreasing the force at z_0 and increasing the liquid volume of the meniscus. For a higher

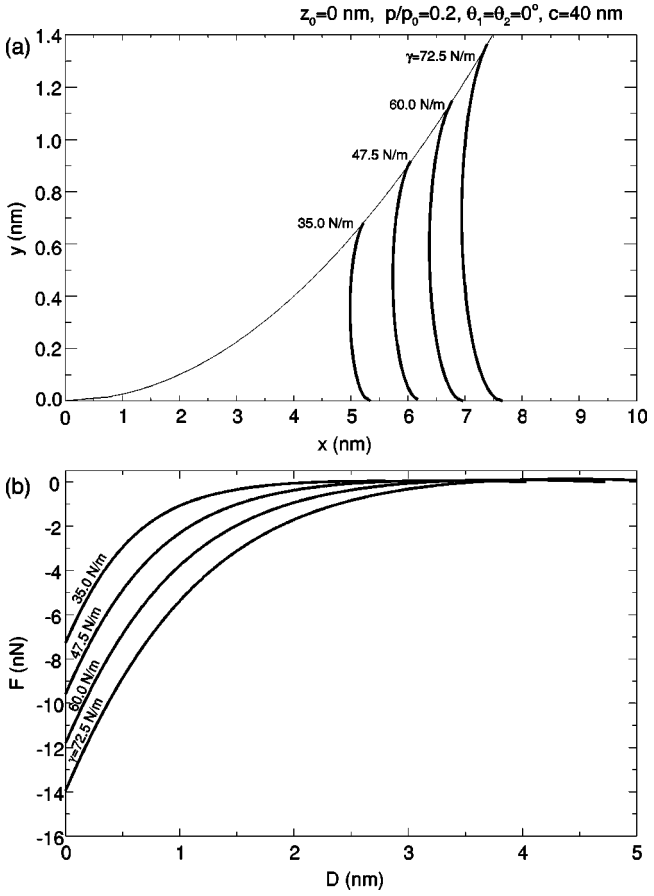

FIG. 3. (a) The upper diagram shows the geometric shape of the meniscus for $D=0$ nm for various surface tensions γ and (b) the lower diagram shows the meniscus force between the tip and surface.

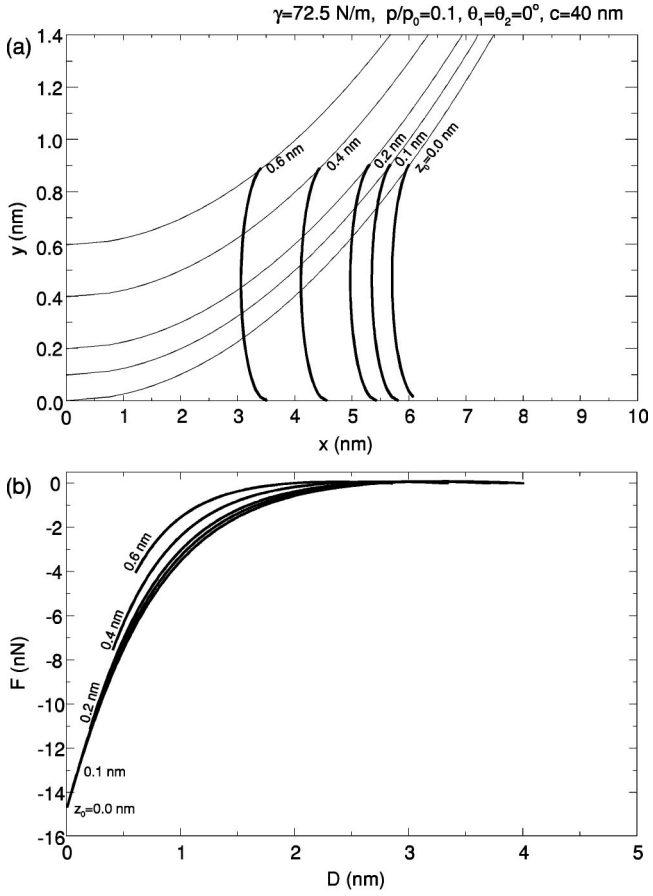

FIG. 4. (a) The upper diagram shows the geometric shape of the meniscus for $D=0$ nm for various z_0, and (b) the lower diagram shows the meniscus force between the tip and surface. In (a) for each z_0 value the tip position is drawn (thin lines).

volume the meniscus can be formed at higher tip-sample distances and therefore the force disappears later. The lower force at z_0 and the disappearance at greater distances explains the weaker distance dependency.

The influence of the surface tension γ on the force curve is presented in Fig. 3. The surface tension appears both in the force equation (9) and in the Kelvin radius equation (3). In both the force and the Kelvin radius equations the surface tension is a scaling factor. In both cases a lower surface tension generally reduces the meniscus force. Due to the smaller Kelvin radius the liquid volume is smaller and the force thus disappears at smaller distances.

In Fig. 4 the effect of different starting separations between tip and sample is shown. With greater z_0 the force at z_0 decreases and the disappearance occurs at greater values of D. The shifting of the disappearance point can again be explained by the greater liquid volume. The lower starting force is caused by a smaller meniscus neck for higher z_0 values.

Figure 5 shows the change due to different tip parameters. With increased tip width the forces are increased, due to greater menisci. A greater tip width means the shape of the meniscus is at a larger distance from the rotation axis. Therefore the pressure difference due to the meniscus acts over a greater area and increases the resulting force. The disappearance point is also shifted to larger distances between tip and surface due to the greater amount of liquid contributing to the meniscus.

The effects of two contact angles at the tip and at the sample and the geometric shape of the meniscus on the meniscus forces are shown in Figs. 6 and 7. In Fig. 6 the contact angle θ_1 at the sample is varied. An increasing angle decreases the meniscus force at z_0 and shifts the disappearance point to smaller separations. The reason for this is due to the smaller amount of liquid contributing to the meniscus, because the Kelvin radius does not change so much. For angles a little greater than 90° no arc satisfying the border condition is found and no meniscus force exists.

The meniscus force for different contact angles θ_2 at the tip is drawn for $\theta_1=0°$ in Fig. 7. The behavior is similar to that determined for the contact angle θ_1 at the sample. With increasing angle the force at z_0 decreases and the disappearance point shifts to lower values. For this case, however, the limit angle for the existence of meniscus forces is lower. For contact angles greater than $\theta_2^{limit}=75.3°$ a meniscus force is no longer valid. For greater sample contact angles θ_1 this limit angle increases. For example, for $\theta_1=80°$ θ_2^{limit} yields 84.1°.

Figure 8 shows the change in geometric shape of a meniscus after retracting the tip from the surface. The parameters are $z_0=0$ nm, humidity $p/p_0=0.2$, contact angle $\theta_1=\theta_2=0°$, and surface tension $\gamma=72.5$ mN/m. At the beginning of the retraction the decrease in force is mainly caused by the decrease of y_0, reducing the area at which the pressure

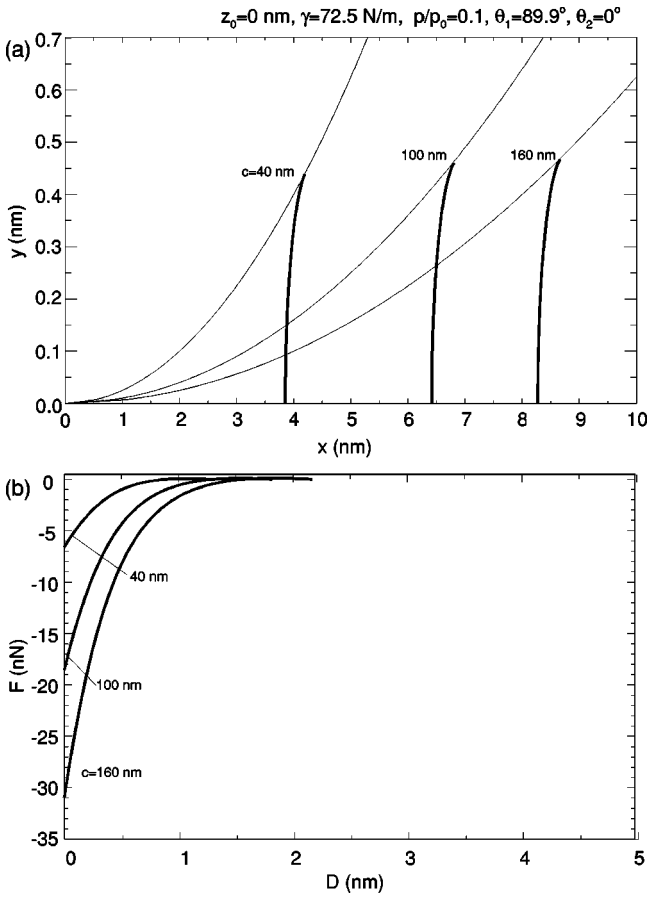

FIG. 5. (a) The upper diagram shows the geometric shape of the meniscus for $D=0$ nm for various tip parameters c, and (b) the lower diagram shows the meniscus force between the tip and surface.

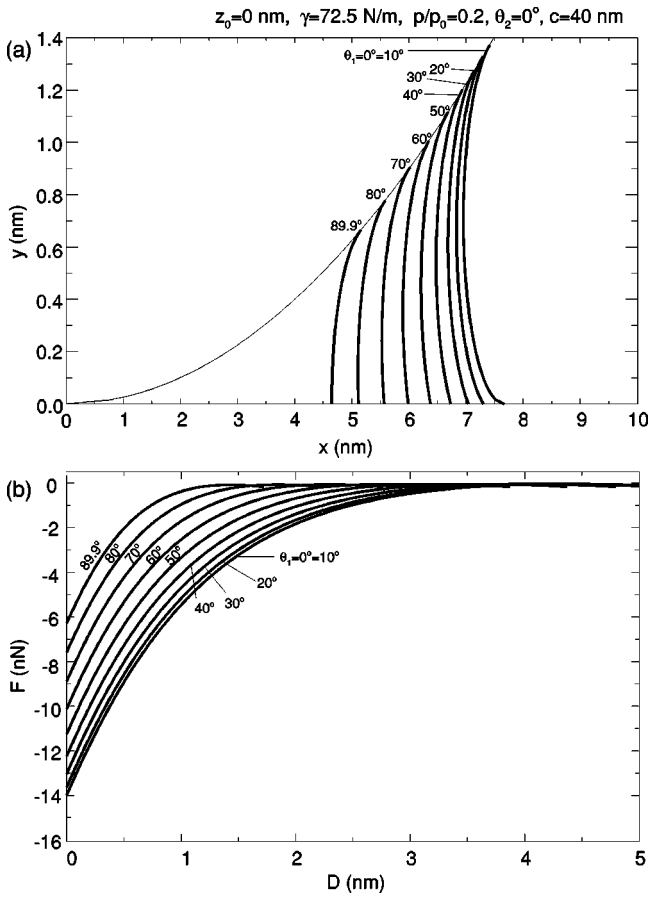

FIG. 6. (a) The upper diagram shows the geometric shape of the meniscus for $D=0$ nm for various contact angles θ_1, and (b) the lower diagram shows the meniscus force between the tip and surface.

due to the meniscus acts. At the end of the retraction, before the meniscus breaks, the change of r_1 is greater, but the value is now quite comparable to y_0. Due to this the radius $r_2=y_0-r_1$ dominates the strength of the meniscus force before the break.

The force curves shown cannot generally be used for the interpretation or calculation of force versus distance curves or pulsed force mode (PFM) curves. One motive for such investigations is that the tip motion influences the meniscus, which must be controlled. An important condition is the break of the meniscus. This could happen much earlier, due to the tensile strength of the liquid. This value is dependent on the velocity in retracting the tip from the surface.

B. van der Waals forces

The two dashed curves in Fig. 9 indicate the spread of possible van der Waals forces for a SFM system.[22] The dotted curve shows the Lennard-Jones force with the strongest van der Waals force. The two solid curves are capillary forces from Fig. 2 indicating the range for different humidities. Comparing both forces shows a weaker distance dependance of the capillary forces. Therefore the capillary forces can be stronger or weaker than van der Waals forces for distances smaller than about 0.5 nm. For greater distances the capillary forces are stronger than the van der Waals forces. van der Waals forces must be considered for a tip-sample distance up to a few nanometers ($D<5$ nm). For many material combinations a smaller tip-sample distance (<2 nm) is enough. Capillary forces operate up to the break of the meniscus. This is shown in Figs. 2 to 7 from 5 nm to 20 nm. For the adhesion force, however, the tip-sample contact and the strength of the interaction for tip-sample separations smaller than 1 nm are important. Thus for large separations for the retraction only the capillary force is necessary, while for smaller separations both forces must be considered. The capillary forces shown here suggest that they are for most cases stronger or combarable to van der Waals forces. However, weaker surface tensions and other contact angles can reduce the strength of the capillary forces.

In Fig. 10 the tip radius dependence is investigated. The forces show a similar increase with increase of tip radius. For the van der Waals force the increase is exactly linear with the tip radius [see Eq. (11)]. The capillary forces shown here are the one of the strongest for each tip radius, together with the strongest van der Waals forces.

IV. CONCLUSIONS

Capillary and meniscus forces between a paraboloid tip and a sample are calculated for various tip geometries, relative humidity, surface tensions, and contact angles. Comparing the van der Waals and the meniscus forces, three possible arrangements can occur. The van der Waals force can be

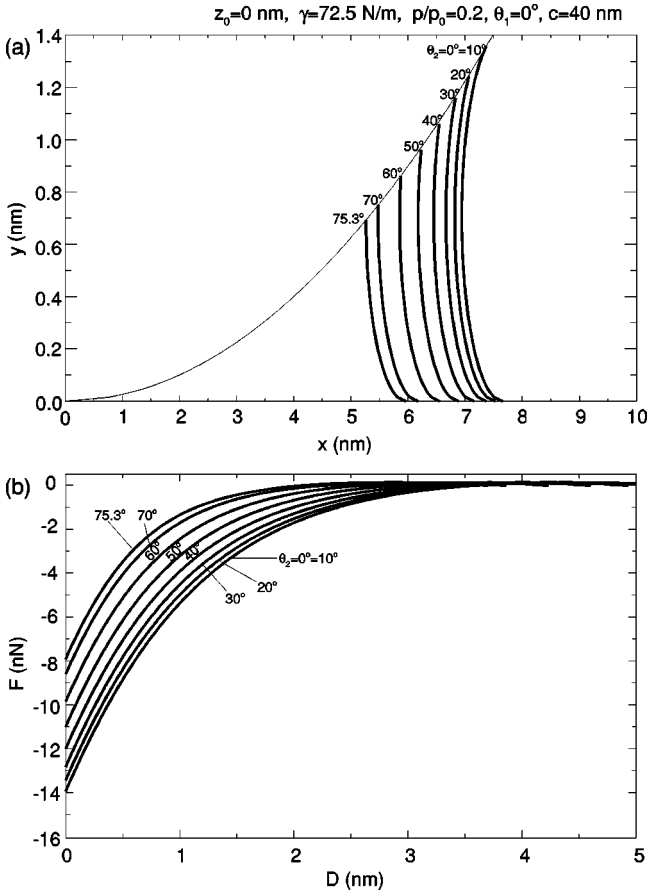

FIG. 7. (a) The upper diagram shows the geometric shape of the meniscus for $D=0$ nm for various contact angles θ_2, and (b) the lower diagram shows the meniscus force between the tip and surface.

dominant, the meniscus force can be dominant, or both forces can be roughly equal. Capillary forces can be minimized by tip geometry or material design. These needs to be minimized for devices with as smooth surfaces and that operate under light loads such as MEMS. A typical problem for MEMS is the sticking of parts on the substrate after, e.g., cleaning processes. If the closest sticking part to the surface has a small effective radius, the strength of the capillary

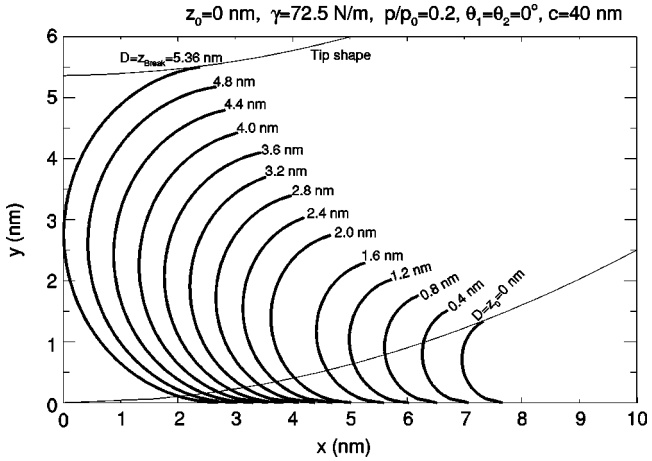

FIG. 8. Change of the meniscus shape by retracting the tip from the surface.

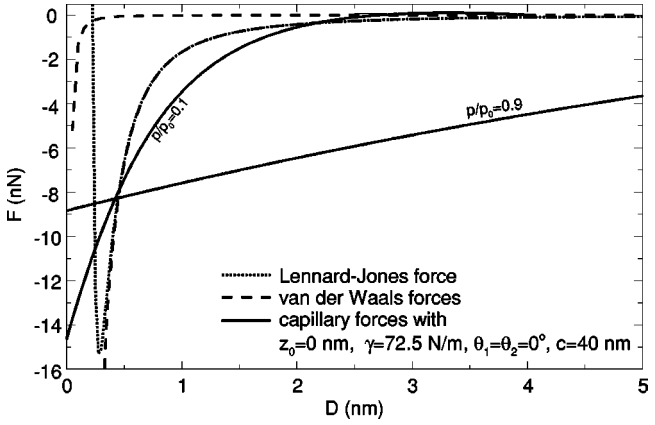

FIG. 9. Comparison of van der Waals and capillary forces. Values for the van der Waals curves (dashed): tip width 20 nm; Hamaker constants 0.04 and 3.0×10^{-19} J. The dotted curve is a Lennard-Jones force with the strongest van der Waals force. The capillary forces show the range for different humidities.

force can be small enough such that the part detaches itself at low humidity. Another problem occurring for MEMS is the intersolid adhesion. This effect can be caused by previously existing capillary forces and can also be reduced or neglected with the aforementioned description. The covering of the tip or the sample with a hydrophobic material reduces the contact angle and therefore the force. The thickness of the hydrophobic material can be very small, which implies that the main contribution of the Lennard-Jones force comes from the material under the hydrophobic layer. This allows us to influence the strength of the Lennard-Jones force through the choice of the tip material.

Further studies and extensions of the model could help especially in determining the real influence of the SFM on the measured properties. The possibility of separating the desired properties from the capillary-force-affected signal could also be explored.

ACKNOWLEDGMENTS

The authors would like to thank H.-U. Krotil and C. S. Imhof (University of Ulm) and T. Kriewall (Department of

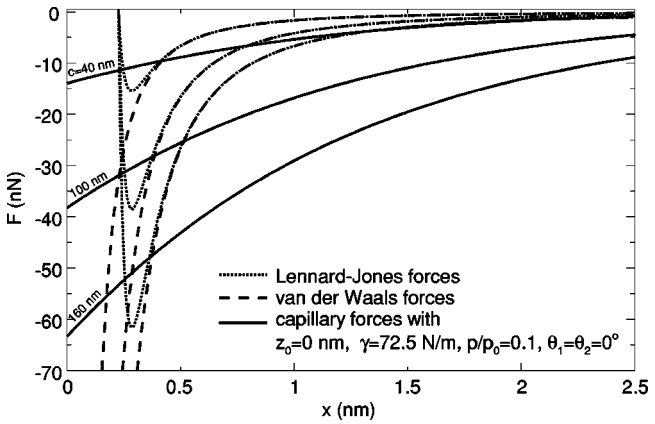

FIG. 10. Comparison of van der Waals and capillary forces for different tip radii. Hamaker constant for the van der Waals forces (dashed): 3.0×10^{-19} J. The dotted curves are Lennard-Jones forces with the corresponding van der Waals forces.

Bioengineering, University of Washington, Seattle) for valuable discussions and comments. This research was supported by Deutsche Forschungsgemeinschaft (DFG) with the priority program ''Grundlagen der elektrochemischen Nanostrukturierung'' Grant No. Ma 1297/5-1 and /5-2. The last author (B.B.) acknowledges financial support from the Alexander von Humboldt Foundation, Bonn Germany, and for a faculty sabbatical leave from The Ohio State University.

*Present address: Visual Analysis GmbH, Neumarkter Str. 87, D-81673 Muenchen, Germany. Email: thomas.stifter@visualanalysis.com

[1] G. Binnig, C.F. Quate, and C. Gerber, Phys. Rev. Lett. **56**, 930 (1986).
[2] B. Bhushan, *Handbook of Micro/Nanotribology*, 2nd ed. (CRC Press, Boca Raton, FL, 1999).
[3] B. Bhushan, *Principles and Application of Tribology* (Wiley, New York, 1999).
[4] J.B. Pethica and D. Tabor, Surf. Sci. **89**, 182 (1989).
[5] C. Schonenberger and S.F. Alvarado, Phys. Rev. Lett. **65**, 3162 (1990).
[6] Y. Martin and H.K. Wickramasinghe, Appl. Phys. Lett. **50**, 1455 (1987).
[7] Y. Sugawara, M. Otha, T. Konishi, and S. Morita, Wear **168**, 13 (1993).
[8] T. Thundat, X.-Y. Zheng, G.Y. Chen, and R.J. Warmack, Surf. Sci. Lett. **294**, L939 (1998).
[9] B. Bhushan and S. Sundararajan, Acta Mater. **46**, 3793 (1998).
[10] K.O. Van der Werf, C.A.J. Putman, B.G. Groth, and J. Greve, Appl. Phys. Lett. **65**, 1195 (1994).
[11] A. Rosa, E. Weilandt, S. Hild, and O. Marti, Meas. Sci. Technol. **8**, 1333 (1997).
[12] H.-U. Krotil, T. Stifter, H. Waschipky, K. Weishaupt, S. Hild, and O. Marti, Surf. Interface Anal. **27**, 336 (1999).
[13] P.J. dePablo, J. Colchero, A.M. GomezHerrero, and J. Baro, Appl. Phys. Lett. **73**, 3300 (1998).
[14] C.H. Mastrangelo and C.H. Hsu, J. Microelectromech. Syst. **2**, 33 (1993).
[15] C.H. Mastrangelo and C.H. Hsu, J. Microelectromech. Syst. **2**, 44 (1993).
[16] J. N. Israelachvili, *Intermolecular and Surface Science*, 2nd ed. (Academic Press, London, 1991).
[17] S.K. Chilamakuri and B. Bhushan, J. Appl. Phys. **86**, 4649 (1999).
[18] T. Stifter, E. Weilandt, O. Marti, and S. Hild, Appl. Phys. A: Mater. Sci. Process. **66**, S597 (1998).
[19] J. Ruan and B. Bhushan, J. Appl. Phys. **76**, 5022 (1994).
[20] J.L. Hutter and J. Bechhoefer, J. Appl. Phys. **73**, 4123 (1993).
[21] J. Colchero, Ph.D. Dissertation, Konstanz: Hartung-Gorre, 1993.
[22] L. Bergstrom, Adv. Colloid Interface Sci. **70**, 125 (1997).